Thermal expansion, phase diagrams and barocaloric effects in $(NH_4)_2NbOF_5$

2010 J. Phys.: Condens. Matter 22 185901

(http://iopscience.iop.org/0953-8984/22/18/185901)

J. Phys.: Condens. Matter **22** (2010) 185901 (8pp) doi:10.1088/0953-8984/22/18/185901

Thermal expansion, phase diagrams and barocaloric effects in $(NH_4)_2NbOF_5$

Michail Gorev[1,2], Evgeny Bogdanov[1], Igor Flerov[1,2] and Nataly Laptash[3]

[1] L V Kirensky Institute of Physics, Siberian Division, Russian Academy of Sciences, Akademgorodok, Krasnoyarsk, 660036, Russia
[2] Institute of Engineering Physics, Siberian Federal University, av. Svobodny 79, Krasnoyarsk, 660041, Russia
[3] Institute of Chemistry, Far Eastern Division, Russian Academy of Sciences, Vladivostok, 690022, Russia

E-mail: gorev@iph.krasn.ru

Received 3 November 2009, in final form 15 March 2010
Published 15 April 2010
Online at stacks.iop.org/JPhysCM/22/185901

Abstract
The thermal expansion along the a, b and c axes of a $(NH_4)_2NbOF_5$ crystal was measured from 120 to 300 K. Anomalies of $\alpha(T)$ associated with previously reported phase transitions $Cmc2_1 \rightarrow C2 \rightarrow Ia$ were observed along all directions at $T_1 = 259.3$ K and $T_2 = 220.5$ K. The analysis of thermal expansion and heat capacity in the frame of the Pippard relations has permitted us to determine the uniaxial pressure derivatives of the transition temperatures $dT/d\sigma_i$. The T–σ_i phase diagrams have shown a tendency for the intermediate phase to disappear at high stress along the b and c axes. Intensive and extensive barocaloric effects near the structural phase transitions were found to be comparable with the caloric parameters of some ferroelectrics, ferromagnets and antiferromagnets.

1. Introduction

The interest in crystals with quasi-octahedral anions containing mixed ligands, in particular oxygen and fluorine atoms, is due to many reasons. First of all, the polar noncentrosymmetric ions $[MO_xF_{6-x}]^{n-}$ (M = Nb, Mo, W, Ti, ...; $x = 1$, 2, 3) make possible, in principle, various polar structures, possessing practically important properties such as pyro-, ferro- and piezoelectricity, second harmonic generation and so on [1]. However, due to the statistical disordering of ligands, many compounds crystallize in centrosymmetric space groups.

A great number of investigations are dedicated to searching for and developing criteria for the design of polar oxyfluorides. Some of them are related to studies of compounds with $[NbOF_5]^{2-}$ ions and organic cations [2, 3]. All inorganic oxyfluorides of the A_2NbOF_5 series with the atomic cations A = Li [4], Na [5], K [6] and Cs [7] crystallize in centrosymmetric space groups with a disordering of oxygen and fluorine ions. Second harmonic generation and a noncentrosymmetric structure with an ordered orientation of distorted octahedra $[NbOF_5]^{2-}$ was revealed only in $KNaNbOF_5$ [3].

Previous studies were performed only at room temperature, and information about the stability and possible structural transformations has been absent up to now. Meanwhile, an investigation of the orientational ordering as a result of phase transitions can provide additional information useful for the creation of polar compounds with the required properties. Only recently was a study of the ammonia compound $(NH_4)_2NbOF_5$ performed over a wide range of temperatures [8, 9]. The detailed study of the heat capacity and T–p phase diagram of $(NH_4)_2NbOF_5$ [8] has shown that this crystal exhibits a sequence of two phase transitions at $T_1 = 258.0$ K and $T_2 = 218.9$ K, accompanied by large entropy changes $\Delta S \approx R \ln 12 + R \ln 8$. Hydrostatic pressure leads to a linear decrease in the transition temperatures of both transformations with the same pressure coefficients $dT_1/dp = -45.4$ K GPa^{-1} and $dT_2/dp = -45.2$ K GPa^{-1}. The structural distortions at the phase transitions are associated with the orientational ordering of both distorted $[NbOF_5]^{2-}$ octahedra and ammonium tetrahedra [8, 9]. According to [9] all three phases are noncentrosymmetric ($Cmc2_1$, $C2$, Ia).

In this work we studied the anisotropic thermal expansion of $(NH_4)_2NbOF_5$ with the aim to obtain additional information about phase transitions and to determine some thermodynamic parameters to clarify the influence of uniaxial stress on the phase transition sequence and barocaloric efficiency.

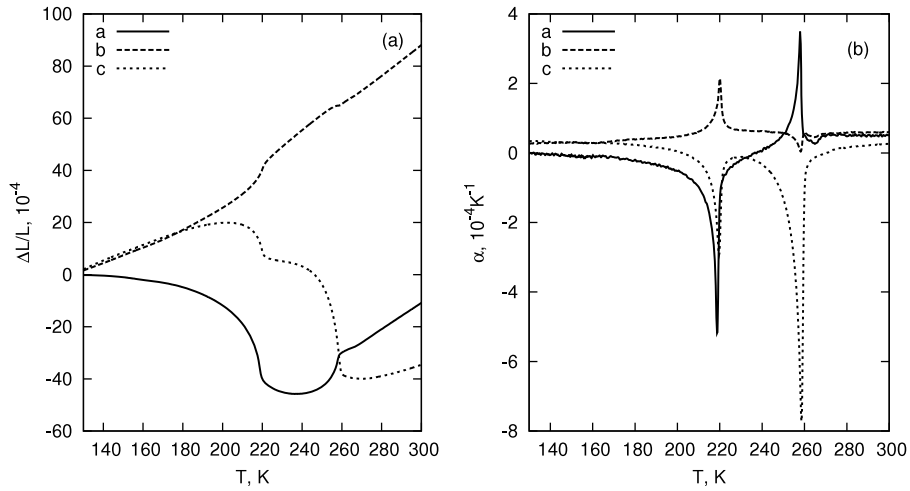

Figure 1. Linear thermal expansion $\Delta L/L$ (a) and thermal expansion coefficients α (b) as functions of temperature for the a, b and c directions.

Oxyfluorides with polar quasi-octahedral ionic groups in the structure are characterized by a high degree of disorder in the initial phase and very large values of entropy change at the phase transitions. These properties, and the high-pressure sensitivity of the transition temperatures, make these compounds very promising for the investigation of the barocaloric effect and its application to solid state refrigeration systems. This new method for adiabatic cooling by the application of pressure was recently proposed by Müller *et al* [10] and Strässle *et al* [11]. Like other adiabatic cooling techniques, barocaloric refrigeration results from an entropy change in the system under investigation. Unlike the well known magnetocaloric and electrocaloric methods, the entropy change does not result from the application of an external magnetic or electric field, but from the application of external hydrostatic pressure or uniaxial stress. The barocaloric effects were estimated near the structural phase transitions in oxyfluoride $(NH_4)_2NbOF_5$ using data from the heat capacity at atmospheric pressure, and temperature–hydrostatic pressure (T–p) and temperature–uniaxial stress (T–σ) phase diagrams.

2. Sample preparation and thermal expansion measurements

Oxyfluoride $(NH_4)_2NbOF_5$ was prepared in a single crystal form as tetrahedral prisms or polyhedra by slow evaporation of the solution. A detailed description of the substance synthesis and crystal growth procedure can be found elsewhere [9]. The samples were cut and polished so as to have parallel surfaces perpendicular to the a, b and c crystallographic directions with distances L between the surfaces equal to 1.583 mm, 5.030 mm and 7.130 mm, respectively.

Thermal expansion measurements were performed in the temperature range 120–300 K with a heating rate of 3 K min^{-1} using a NETZSCH model DIL-402C push-rod dilatometer with a fused silica sample holder. The results were calibrated, by taking SiO_2 as the standard reference, to remove the influence of system thermal expansion.

3. Results and discussion

3.1. Thermal expansion

Anisotropic and temperature dependent linear ($\Delta L/L$) and volume ($\Delta V/V$) thermal expansions as well as thermal expansion coefficients (α along a, b and c directions and β) of $(NH_4)_2NbOF_5$ are shown in figures 1 and 2. The changes of ΔL and ΔV are taken relative to the L and V values at 120 K. In accordance with the orthorhombic symmetry of $(NH_4)_2NbOF_5$ the volume expansion coefficient was calculated as $\beta = \alpha_a + \alpha_b + \alpha_c$. The results of several series of measurements correlate well with each other.

All linear thermal expansion coefficients α_a, α_b and α_c show two anomalies, at $T_1 = 259.3$ K and $T_2 = 220.5$ K, related to the phase transitions $Cmc2_1 \rightarrow C2 \rightarrow Ia$ observed in [8, 9]. Both values T_1 and T_2 are slightly higher than obtained by heat capacity [8], which is a result of the dynamic nature of thermal expansion measurements.

Near the phase transition at T_2 as the temperature increases the sample size decreases along the a and c directions and increases along the b direction. At T_1 the sample size continues to decrease along the b and c directions and increases along a axis (figure 1). Nevertheless the volume of the sample is decreased at both T_1, and T_2 (figure 2).

Correct extraction of the anomalous contributions to the strain is a very important point for the data analysis. We have tried to carry out this procedure by several methods. Firstly, similar to a traditional approach we approximated the $\Delta V/V$ data at high temperatures $T > T_1$ by a straight line. But the results are poorly defined, as we detect some deviations from the linear temperature dependence of strain, and variation of the thermal expansion coefficients $\alpha(T)$ and $\beta(T)$. The temperature at which nonzero anomalous strain contributions arise, and their values at $T < T_1$, depend appreciably on the range in which the high temperature data are fitted.

The coefficients $\alpha_i(T)$ show a nearly linear temperature dependence at $T > T_1$ and we try to approximate the regular thermal expansion coefficients by linear equations.

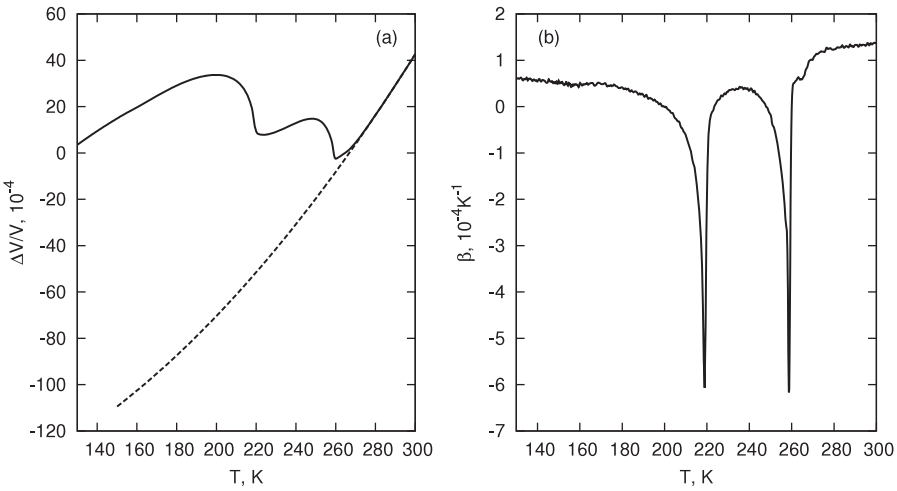

Figure 2. Temperature dependencies of relative volume change (a) and volume thermal expansion coefficient (b) of $(NH_4)_2NbOF_5$.

Accounting for these contributions considerably improves the approximations of the temperature dependencies of $\alpha_i(T)$ and $(\Delta L/L)(T)$ at $T > T_1$ and reduces the values of anomalous strain in the low temperature region. As the temperature is decreased the thermal expansion coefficients should tend to zero, and in the low temperature region ($T < T_1 < \Theta_D$, where Θ_D is Debye temperature) it is necessary to consider the relation between thermal expansion and heat capacity, and the $C_p(T)$ function, at least within the Debye model. The results of such an approximation of $\Delta V/V$ are shown by the dashed line in figure 2(a).

3.2. Clausius–Clapeyron and Pippard relations

Considerable evidence for the first order nature of both structural phase transitions in $(NH_4)_2NbOF_5$ was obtained in calorimetric studies [8]. A significant hysteresis in the phase transition temperatures ($\delta T_1 = 0.63$ K; $\delta T_2 = 1.04$ K) and jumps in the enthalpy ($\delta H_1 = 710$ J mol^{-1}; $\delta H_2 = 480$ J mol^{-1}) as well the entropy ($\delta S_1 = \delta H_1/T_1 = 2.8$ J mol^{-1} K^{-1}; $\delta S_2 = \delta H_2/T_2 = 2.2$ J mol^{-1} K^{-1}) were revealed in carefully measured quasi-static thermograms with $|dT/dt| \approx 0.02$ K min^{-1}.

According to the data above, the pressure dependencies of T_1 and T_2 can be calculated using the Clausius–Clapeyron equation

$$\frac{dT_0}{dp} = \frac{\delta V}{\delta S}, \qquad (1)$$

where δV and δS are the discontinuous volume and entropy changes at the phase transition temperature, respectively. Unfortunately, we were unable to determine exactly the jumps of the elongation and the volume at the transition temperatures, because both transformations are very close to the tricritical point [8]. Moreover thermal expansion anomalies near the phase transition temperatures are smeared out due to the dynamic nature of thermal expansion measurements, thus leading to significant errors in the volume jump determination. The estimation of the pressure derivatives of the transition temperatures using total entropy (ΔS_1, ΔS_2) and volume (ΔV_1, ΔV_2) changes give values $dT_1/dp \approx dT_2/dp \approx -32$ K GPa^{-1}; much less than the experimental values [8].

For a more accurate determination of dT/dp one can use the Pippard relations [12], which connect the thermal expansion coefficients and the specific heat near the phase transition temperature

$$C_p = \frac{V_m T_0}{\gamma_i}\alpha_i + \text{const}, \qquad C_p = \frac{V_m T_0}{\gamma}\beta + \text{const}, \qquad (2)$$

where C_p—heat capacity, V_m—molar volume, T_0—phase transition temperature,

$$\gamma_i = \left(\frac{\partial T_0}{\partial \sigma_i}\right)_{\sigma_j, j\neq i}, \qquad \gamma = \frac{dT_0}{dp} = \sum_i \gamma_i. \qquad (3)$$

The value of the molar volume is equal to $V_m = 938.56 \times 10^{-7}$ m^3 mol^{-1} according to structural data [9]. Equations (2) allow the calculation of both dT_0/dp and $dT_0/d\sigma_i$ values and the construction of the temperature–uniaxial stress phase diagrams.

Hereinafter the temperature dependence of heat capacity obtained by adiabatic calorimetry [8] was used. Because the values of dT/dp and $dT/d\sigma_i$ strongly depend on the data closest to the critical temperatures, slight errors in the temperature scales of measurements of heat capacity by adiabatic calorimeter (temperature sensor—platinum thermometer) [8] and thermal expansion by dilatometer (temperature sensor—thermocouple) will produce significant errors in the results calculated from the Pippard theory. In this case the data on thermal expansion and heat capacity have been brought to one temperature scale by alignment of the phase transition temperatures.

The results of combined analysis of the thermal expansion and molar heat capacity below T_1 and T_2 are shown in figures 3 and 4, respectively. The experimental points for both β and α_i fall on straight lines. That means the Pippard relations (2) hold for both phase transitions in the temperature ranges 2.5–12 K and 2–10 K below the transition temperatures T_1 and T_2.

Deviations from relations (2) are observed in the vicinity of transition temperatures $T_1 - T < 2.5$ K and $T_2 - T < 2$ K,

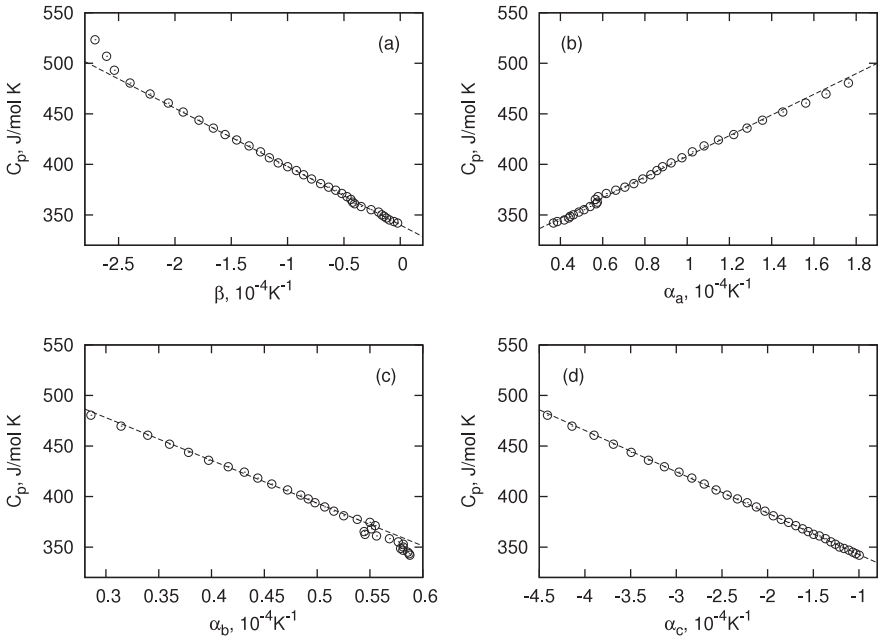

Figure 3. Molar heat capacity C_p versus volume β (a) and linear α_i ((b)–(d)) thermal expansion coefficients plot of $(NH_4)_2NbOF_5$ below T_1.

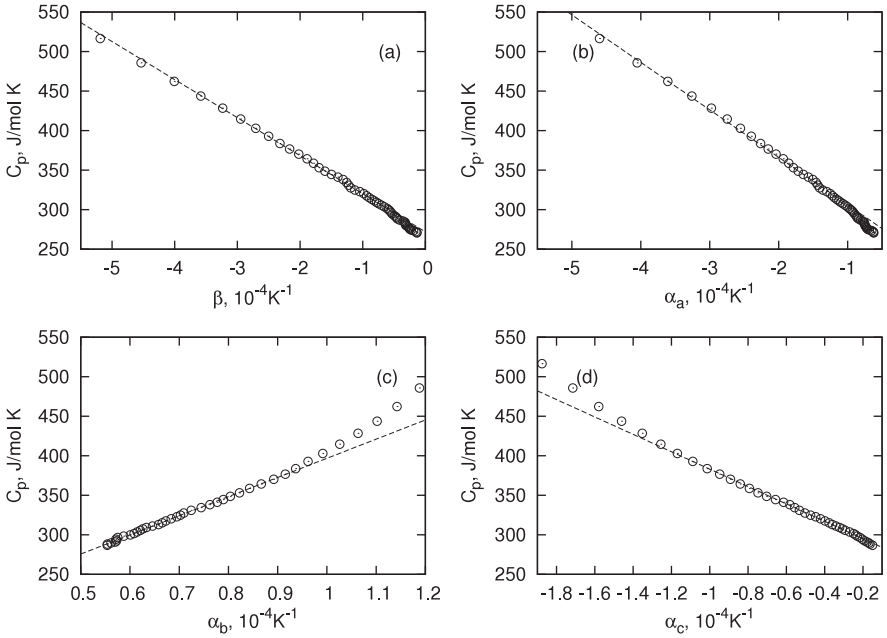

Figure 4. Molar heat capacity C_p versus volume β (a) and linear α_i ((b)–(d)) thermal expansion coefficients plot of $(NH_4)_2NbOF_5$ below T_2.

where the effects of the imperfections of the samples, dynamic nature of thermal expansion measurements and the difference of temperature scales for C_p and α measurements are most significant.

Experimental values [8] and values calculated from the Pippard relations (2) of $\gamma = \mathrm{d}T/\mathrm{d}p$ and $\gamma_i = \mathrm{d}T/\mathrm{d}\sigma_i$ are presented in table 1. The calculated values of $\mathrm{d}T/\mathrm{d}p$ correspond well with the experimentally determined temperature–pressure phase diagram [8]. The agreement of experimental $\mathrm{d}T/\mathrm{d}p$ and calculated $\sum_i \gamma_i$ gives us hope that the values of γ_i are close to real ones as well.

3.3. Phase diagrams

The results of $\mathrm{d}T/\mathrm{d}p$ and $\mathrm{d}T/\mathrm{d}\sigma_i$ calculations allow us to construct the T–p and T–σ_i phase diagrams (figure 5). One can see that the main effect on the phase transition sequence is connected with mechanical stress along the a and c directions. The σ_a stress stabilizes the intermediate distorted phase, contrary to the effect of the σ_c stress, which results in a rather rapid narrowing of $C2$ phase range and the existence of a triple point at $\sigma_c \approx 0.95$ GPa. The temperature range of the intermediate phase stability also narrows as σ_b increases, but the triple point is observed at a significantly higher value of σ_b.

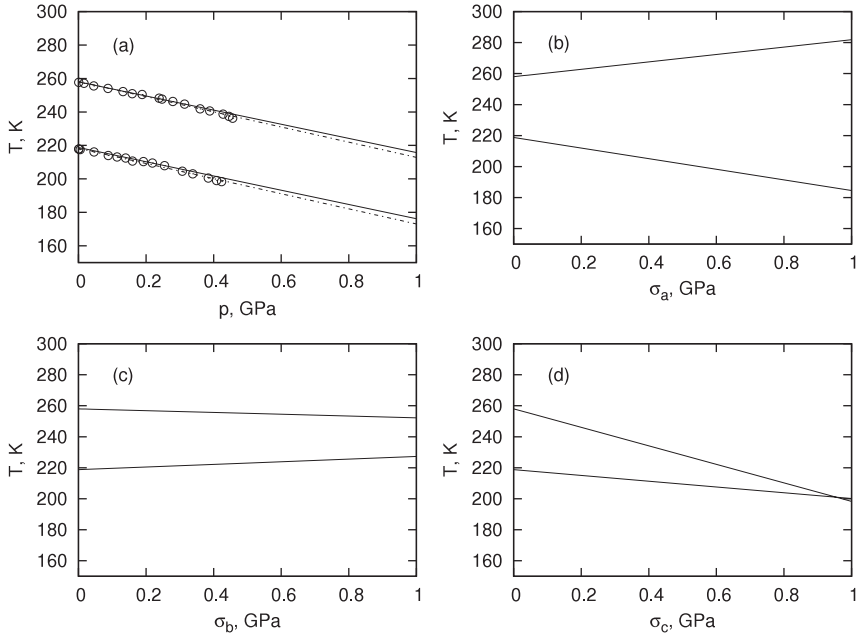

Figure 5. T–p (a) and T–σ ((b)–(d)) phase diagrams of $(NH_4)_2NbOF_5$. O and - - - - experimental data [8], —— calculated by the Pippard relations.

Table 1. Experimental [8] and calculated values of pressure and stress dependencies of the phase transition temperatures.

	Phase transition at T_1		Phase transition at T_2	
	Experimental	Calculated	Experimental	Calculated
γ (K GPa^{-1})	−45.4	−42.3	−45.2	−42.7
$\gamma_a + \gamma_b + \gamma_c$ (K GPa^{-1})	−45.4	−41.6	−45.2	−44.4
γ_a (K GPa^{-1})		23.9		−34.2
γ_b (K GPa^{-1})		−5.8		8.5
γ_c (K GPa^{-1})		−59.7		−18.7

3.4. Barocaloric effect

All adiabatic cooling techniques are based on the same thermodynamic principle and hence suffer the same general thermodynamic restrictions. They make use of the fact that the total entropy S of a system is a thermodynamic state function and thus depends on external thermodynamic variables (temperature T, pressure p, electric E and magnetic H fields) $S = S(T, p, E, H)$. Upon an isothermal change of external pressure there is the extensive barocaloric effect $\Delta S_{\mathrm{BCE}}(T, p) = S(T, p) - S(T, 0)$. The adiabatic change of external pressure leads to a change in temperature ΔT_{AD} (intensive barocaloric effect) as the total entropy must be conserved $S(T + \Delta T_{\mathrm{AD}}, p) = S(T, 0)$.

Different methods for the measurement of the intensive caloric effect ΔT_{AD} are used, but the most reliable device for these purposes is the adiabatic calorimeter, which makes it possible to regulate and to actually minimize the heat exchange with the environment, providing the adiabatic conditions for the experiment $S = \mathrm{const}$. From calorimetric studies, in principle, it is also possible to obtain information about the extensive caloric effect by measurements of the heat capacity of materials as a function of temperature and the field of corresponding nature.

Unfortunately, the adiabatic calorimeter is unsuitable practically for the studies of barocaloric effect caused by hydrostatic pressure, since in this case it is necessary to use a massive high-pressure chamber with a suppressed contribution of heat capacity to the experimentally measured heat capacity (chamber + sample). As a consequence there is a significant loss in the accuracy of the heat capacity determination of the sample (and, correspondingly, the entropy) which makes the determination of $\Delta T_{\mathrm{AD}}(p)$ and ΔS_{BCE} impossible practically.

Alternative indirect methods based on Maxwell's equations are frequently used for the determination of the extensive magnetocaloric and electrocaloric effects by using data on the dependencies of the generalized coordinate (magnetization, polarization) on the temperature and the generalized force (magnetic and electrical field). For precise calculations of barocaloric effects by this strategy it is necessary to obtain information about the equation of state (dependence of volume on the temperature and the pressure), for example, by high-pressure diffraction methods. Unfortunately, such studies have not yet been performed.

In this work we determined the intensive and extensive barocaloric effects using the experimental heat capacity at $p = 0$ and the T–p phase diagram data in a similar way to that earlier done for the magnetic phase transition in

$EuNi_2(Si_{0.15}Ge_{0.85})_2$ [11] and the structural phase transition in oxyfluoride Rb_2KTiOF_5 [13].

Since in the nonferroelectric and nonferromagnetic crystal $(NH_4)_2NbOF_5$ ionic bonds predominate, it is possible to assume that pressure has a basic effect on the behaviour of the anomalous entropy ΔS associated with structural phase transitions. A substantial change in other components of the entropy, including regular lattice entropy S_L, in the investigated range of low pressures, is most probably almost absent. Thus, the lattice entropy, determined at atmospheric pressure, can be used as the background entropy for the analysis of the pressure influence.

The regular lattice component of heat capacity $C_L(T)$ was determined by fitting the experimental data $C_p(T)$, outside the temperature region where the anomalous $\Delta C(T)$ part exists, using a combination of the Debye and Einstein functions [8]. The temperature dependencies of the lattice entropy $S_L(T)$ change in the temperature range investigated (90–340 K) and the anomalous component $\Delta S(T)$ were obtained by integration of the functions $C_L(T)/T$ and $\Delta C/T = (C_p(T) - C_L(T))/T$, respectively. The anomalous entropies $\Delta S_1(T)$ and $\Delta S_2(T)$ of the phase transitions were separated using the approximation of the data near T_2 by the sigmoid $\Delta S_2(T) = a(1 + \exp[(T_2 - T)/b])$.

The entropy for $p > 0$ as a function of temperature and pressure (figure 6) was determined by summation of the pressure independent regular lattice entropy $S_L(T)$ and the anomalous contributions $\Delta S_1(T)$ and $\Delta S_2(T)$ at $p = 0$, shifted along the temperature scale according to the pressure dependencies of the transition temperatures $T_1(p)$ and $T_2(p)$, obtained in [8].

$$S(T, p) = S_L(T) + \Delta S_1\left(T + \frac{dT_1}{dp}p\right) + \Delta S_2\left(T + \frac{dT_2}{dp}p\right). \quad (4)$$

We assume that, in the pressure range under investigation, the hydrostatic pressure does not lead to a significant change in the degree of the proximity of phase transitions to the tricritical points and does not change the numbers of equivalent orientational states of octahedral and tetrahedral ionic groups in the initial and distorted phases, and thus does not change the values of ΔS_1 and ΔS_2.

Figure 7 shows the resulting extensive BCE $\Delta S_{BCE}(T, p) = S(T, p) - S(T, 0)$ and the intensive BCE ΔT_{AD} defined as $S(T, p) = S(T + \Delta T_{AD}, 0)$.

It is obvious that the maximum possible magnitude of the extensive caloric effect is equal to the value of the entropy change associated with both phase transitions, $\Delta S = 37.4$ J mol^{-1} K^{-1}. However, this entropy is divided between two transformations and until $T_2(0) < T_1(p) = T_1(0) + p dT_1/dp$, two separate overlapped peaks of ΔS_{BCE} are observed. At $p > 0.85$ GPa an increase in ΔS is observed.

3.5. Barocaloric effect caused by uniaxial pressure

The serious disadvantage of the barocaloric effect is the massive equipment to produce high hydrostatic pressure. The caloric effect resulting from uniaxial stress variation does not have this disadvantage and is more attractive for applications.

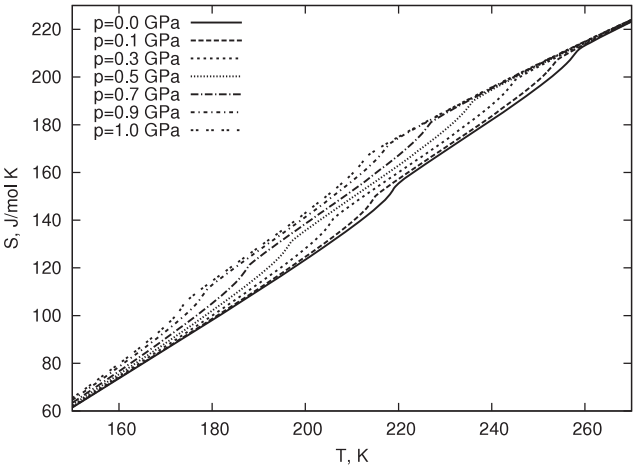

Figure 6. Calculated entropies at different hydrostatic pressures.

The extensive ΔS_{BCE} and the intensive ΔT_{AD} caloric effects caused by uniaxial pressure (figure 8) were estimated in a similar way to the barocaloric effects. The entropy as a function of temperature and stress in this case was determined by the summation of the stress independent lattice entropy $S_L(T)$ and the anomalous components of entropy $\Delta S_1(T)$ and $\Delta S_2(T)$, shifted along the temperature scale according to $T_1(\sigma)$ and $T_2(\sigma)$, obtained from the Pippard relations. It was assumed that neither the uniaxial stresses nor the hydrostatic pressure lead to a significant change in the degree of proximity of the phase transitions to the tricritical points.

In contrast to the hydrostatic pressure the stress along a and b leads to different signs of caloric effects near T_1 and T_2, that are connected to the different signs of the coefficients $dT_1/d\sigma$ and $dT_2/d\sigma$ along these directions. The greatest effects are observed on application of stress along the a and c directions (figures 8(a), (b) (e) and (f)). $dT_1/d\sigma_b$ and $dT_2/d\sigma_b$ are relatively low, which also leads to low values and narrow temperature intervals of the caloric effects ΔS and ΔT (figures 8(c) and (d)).

4. Conclusions

In line with the results of the thermal expansion measurements, the main contribution to the negative volume deformation of the $(NH_4)_2NbOF_5$ crystal lattice is associated with the behaviour of linear deformation along the a and c axes.

The Pippard relations were found to be suitable to describe the relation between the coefficients of the linear and volume expansions and heat capacity in a wide temperature range. There is a good agreement between the values of the baric coefficient dT/dp measured experimentally and calculated using the Pippard equation. The temperature–uniaxial pressure phase diagrams revealed a rather different behaviour of the phase transitions temperatures depending on the direction of the uniaxial stress.

Hydrostatic and uniaxial pressures up to 1 GPa lead to sufficiently high magnitudes of intensive and extensive caloric effects in oxyfluoride $(NH_4)_2NbOF_5$ undergoing order–disorder phase transitions. In accordance with the negative

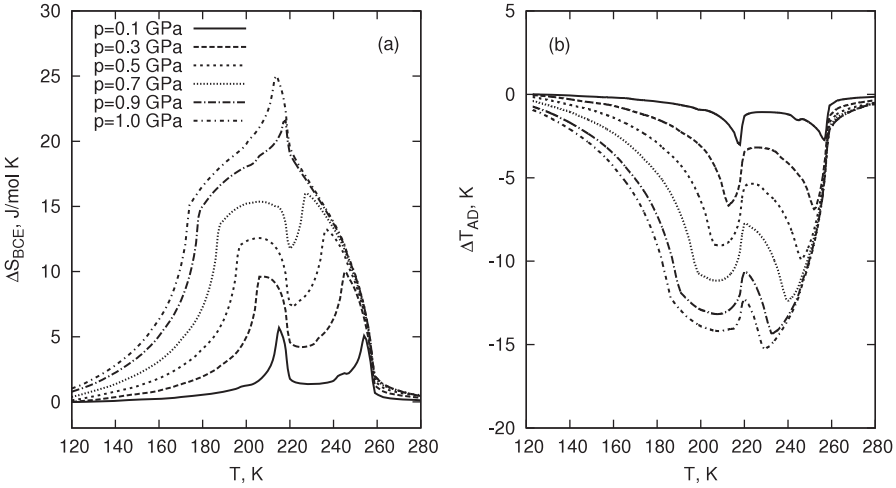

Figure 7. The extensive BCE ΔS_{BCE} (a) and the intensive BCE ΔT_{AD} (b) caloric effects at different pressures.

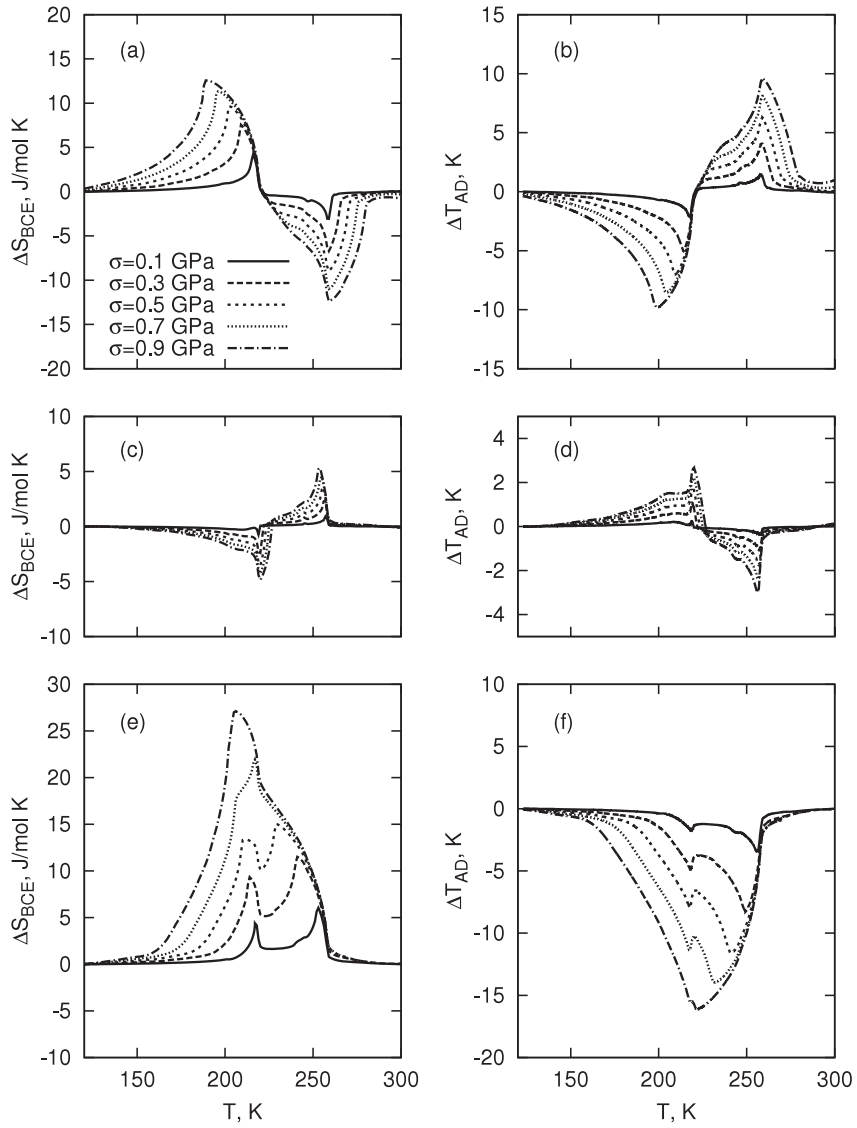

Figure 8. The extensive ΔS_{BCE} and the intensive ΔT_{AD} caloric effects at different values of σ along *a* ((a), (b)), *b* ((c), (d)) and *c* ((e), (f)) directions.

Table 2. Phase transition temperature (T_i) and caloric effects (ΔT_{AD} and ΔS_{CE}) induced by magnetic (H) and electric (E) fields or pressure (p) for some materials.

Material	T_i (K)	ΔT_{AD} (K)	ΔS_{CE} (J kg^{-1} K^{-1})	ΔH (kOe)	ΔE (kV cm^{-1})	p (GPa)	Reference
$(NH_4)_2NbOF_5$	220; 260	−15	60			1	
Rb_2KTiOF_5	215	18	−46			0.56	[13]
CeSb	16	4	−19			0.2–0.5	[11]
$EuNi_2(Si_{0.15}Ge_{0.85})_2$	50	14	−39			0.2–0.5	[11]
MnAs	312	13	−32	50			[14]
$Gd_5Si_2Ge_2$	280	15	−18.5	50			[16]
$PbSc_{1/2}Ta_{1/2}O_3$	290	2.4			138		[15]
$PbZr_{0.95}Ti_{0.05}O_3$	500	15	−8		480		[17]

volume change near the phase transition points the barocaloric effect is an inverse one ($\Delta T_{AD} < 0$, $\Delta S_{CE} > 0$). Table 2 presents data comparing the caloric efficiency of oxyfluoride dielectrics, ferroelectrics and magnets. Taking into account that a comparison of the effects of a different physical nature induced by different fields is quite subjective, it should be nevertheless noted that the oxyfluorides studied here have ΔT_{AD} and ΔS_{CE} exceeding in magnitude known materials regarded as promising refrigerants. Additionally, the ΔT_{AD} value for the oxyfluorides is close to the maximum over a very wide temperature range, unlike the situation with other materials.

Acknowledgments

This work was supported in part by the Krasnoyarsk Regional Foundation for Support of Scientific and Scientific-Technological Investigations and RFBR in the framework of project 'Siberia' (Grant No. 09-02-98001), and the Council on Grants from the President of the Russian Federation for Support of Leading Scientific Schools (project No. Nsh-1011.2008.2).

References

[1] Withers R L, Brink F J, Liu Y and Noren L 2007 *Polyhedron* **26** 290
[2] Izumi H K, Kirsch J E, Stern C L and Poeppelmeier K R 2005 *Inorg. Chem.* **44** 884
[3] Marvel R, Lesage J, Back J, Halasyamani P S, Stern C L and Poeppelmeier K R 2007 *J. Am. Chem. Soc.* **129** 13963
[4] Galy J, Andersson S and Portier J 1969 *Acta Chem. Scand.* **23** 2949
[5] Stomberg R 1984 *Acta Chem. Scand.* **A38** 603
[6] Pinsker G Z 1966 *Kristallografiya* **11** 741
[7] Fourquet J L, Jacobini C and de Pape R 1973 *Mater. Res. Bull.* **8** 393
[8] Fokina V D, Bogdanov E V, Gorev M V, Molokeev M S, Pogoreltzev E I, Flerov I N and Laptash N M 2010 *Phys. Solid State* **52** 781
[9] Udovenko A A and Laptash N M 2008 *Acta Crystallogr.* B **64** 527
[10] Müller K A, Fauth F, Fischer S, Koch M and Furrer A 1998 *Appl. Phys. Lett.* **73** 1056
[11] Strässle T, Furrer A, Hossain Z and Geibel Ch 2003 *Phys. Rev.* B **67** 054407
[12] Pippard A B 1964 *The Elements of Classical Thermodynamics* (Cambridge: Cambridge University Press)
[13] Gorev M V, Flerov I N, Bogdanov E V, Voronov V N and Laptash N M 2010 *Phys. Solid State* **52** 377
[14] Tishin A M and Spichkin Y I 2003 *The Magnetocaloric Effect and its Applications* (*Series in Condensed Matter Physics*) (Bristol: Institute of Physics Publishing)
[15] Shebanov L, Borman K, Lawless W N and Kalvane A 2002 *Ferroelectrics* **273** 137
[16] Gschneidner K A, Pecharsky V K, Pecharsky A O, Ivtchenko V V and Levin E M 2000 *J. Alloys Compounds* **303/304** 214
[17] Mischenko A S, Zhang Q, Scott J F, Whatmore R W and Mathur N D 2006 *Science* **311** 1270